

Diffusion-weighted imaging in the head and neck region: usefulness of apparent diffusion coefficient values for characterization of lesions

Ismail Şerifoğlu, İbrahim İlker Oz, Murat Damar, Özlem Tokgöz, Ömer Yazgan, Zuhale Erdem

PURPOSE

We aimed to evaluate the role of apparent diffusion coefficient (ADC) values calculated from diffusion-weighted imaging for head and neck lesion characterization in daily routine, in comparison with histopathological results.

METHODS

Ninety consecutive patients who underwent magnetic resonance imaging (MRI) at a university hospital for diagnosis of neck lesions were included in this prospective study. Diffusion-weighted echo-planar MRI was performed on a 1.5 T unit with b factor of 0 and 1000 s/mm² and ADC maps were generated. ADC values were measured for benign and malignant whole lesions seen in daily practice.

RESULTS

The median ADC value of the malignant tumors and benign lesions were 0.72×10⁻³ mm²/s, (range, 0.39–1.51×10⁻³ mm²/s) and 1.17×10⁻³ mm²/s, (range, 0.52–2.38×10⁻³ mm²/s), respectively, with a significant difference between them (*P* < 0.001). A cutoff ADC value of 0.98×10⁻³ mm²/s was used to distinguish between benign and malignant lesions, yielding 85.3% sensitivity and 78.6% specificity. The median ADC value of lymphomas (0.44×10⁻³ mm²/s; range, 0.39–0.58×10⁻³ mm²/s) was significantly smaller (*P* < 0.001) than that of squamous cell carcinomas (median ADC value 0.72×10⁻³ mm²/s; range, 0.65–1.06×10⁻³ mm²/s). There was no significant difference between median ADC values of inflammatory (1.13×10⁻³ mm²/s; range, 0.85–2.38×10⁻³ mm²/s) and noninflammatory benign lesions (1.26×10⁻³ mm²/s; range, 0.52–2.33×10⁻³ mm²/s).

CONCLUSION

Diffusion-weighted imaging and the ADC values can be used to differentiate and characterize benign and malignant head and neck lesions.

Diagnosis of head and neck lesions is difficult due to the complicated anatomic structure and different histological components of the many tissues that the neck contains. Imaging of head and neck lesions is not only important for diagnosis of lesions, but also for differentiation of benign lesions from malignant lesions and staging of tumors. While conventional imaging methods mainly evaluate morphological properties, their value is limited in recognizing prognostic characteristics such as benign-malignant differentiation of lesions (1). Routine magnetic resonance imaging (MRI) is a time-consuming method, which is sensitive to differences between examiners and may require the use of contrast material. With development of rapid MRI sequences (such as echo-planar [EPI], fast advanced spin echo [FASE], split echo acquisition of fast spin echo [SPLICE]), the sensitivity to susceptibility artifacts limiting the use of MRI for the head and neck region and limitations linked to duration have been significantly reduced (2, 3).

Diffusion-weighted magnetic resonance imaging (DW-MRI) is a short sequence produced from EPI, FASE, SPLICE sequences. DW-MRI is sensitive to the randomized (Brownian) motion of water molecules at a microscopic level, which provides functional information about tissues. DW-MRI was initially used to diagnose early stroke in the brain and to evaluate brain masses (4–6). Previous studies have shown that rapid growth of high-grade tumors like astrocytoma and lymphoma causes hypercellularity, which leads to limitation of the diffusion of water molecules. Nowadays, apparent diffusion coefficient (ADC) maps calculated from DW-MRI sequences are being increasingly used to provide quantitative data for head and neck lesion diagnosis. In malignant lesions, the DW-MRI signal increases and signal loss is observed on ADC maps (5, 7, 8). Many researchers benefited from this feature of DW-MRI and evaluated the effectiveness of DW-MRI for head and neck lesion identification, benign-malignant differentiation, and characterization of malignant lesions (9–11).

In this prospective study, head and neck lesions that are seen in daily routine were evaluated using DW-MRI, and the role of ADC values in lesion characterization was investigated with the guidance of histopathological results.

Methods

Patients

From January 2012 to January 2014, 90 consecutive patients underwent MRI for diagnosis of head and neck lesions in our center. Among them, 15 patients were excluded due to lack of histopathological results, seven patients were excluded because of motion artifacts, and six patients were

From the Department of Radiology (I.Ş. ✉ driserif@yahoo.com, İ.I.O., Ö.Y. Z.E.), Head and Neck Surgery (M.D.), Bulent Ecevit University School of Medicine, Zonguldak, Turkey, the Department of Radiology (Ö.T.), Abdurrahman Yurtaslan Ankara Oncology Training and Research Hospital, Ankara, Turkey.

Received 2 July 2014; revision requested 28 July 2014; final revision received 31 October 2014; accepted 31 October 2014.

Published online 20 April 2015.
DOI 10.5152/dir.2014.14279

excluded due to lesions that are less than 1 cm in size which do not allow ADC measurements. Final study population included 62 patients (44 men and 18 women; median age, 55 years; range, 18–83 years) who had lesions larger than 1 cm in size and a histopathological diagnosis were included in the study. All patients had good quality ADC maps enabling measurements.

The study protocol conformed to the ethical guidelines of the 1975 Declaration of Helsinki and it was approved by the local ethics committee. Informed consent was obtained from all individuals.

Magnetic resonance imaging techniques

A 1.5 Tesla system (Intera Master Gyrosan, Philips Medical Systems) with a head and neck coil was used for MRI. The routine MRI protocols were used for all patients including transverse T1-weighted turbo spin-echo (TSE) (TR/TE=430/12 ms) and T2-weighted turbo spin-echo (TSE) (TR/TE=4525/100 ms) sequences with or without fat suppression with slice thickness, 6 mm; slice gap, 0.6 mm; field-of-view, 23×25 cm; and matrix size, 228×512.

Diffusion-weighted single-shot EPI MRI was performed before contrast injection at b factor 0 and 1000 s/mm² with the following parameters: TR/TE=4000–4280/94–110 ms; field-of-view, 23×28 cm; matrix size, 94×160; slice thickness, 6 mm; slice gap, 1.2 mm; and bandwidth 2.137 kHz. The spectral presaturation with inversion recovery (SPIR) was used for fat suppression. We did not use any antisusceptibility devices on the head and neck to reduce the susceptibility artifacts; respiratory triggering and cardiac gating were not used.

Next, we obtained T1-weighted turbo spin-echo (TR/TE=430–606/12 ms) in transverse, sagittal, and coronal planes after intravenous injection of gadopentetate dimeglumine (Magnevist, Bayer Pharma AG) in all patients with SPIR for fat suppression with slice thickness, 6 mm; slice gap, 0.6 mm; field-of-view, 23×25 cm; and matrix size, 190×512.

Magnetic resonance imaging analysis

A computer program included in Philips Extended MR Workspace (version 2.6.3.2 Philips Medical Systems)

Table 1. Diagnosis of lesions and locations in the head and neck region

	Diagnosis	Location	
Malignant lesions (n=34)	Squamous cell carcinoma (17)	Larynx (11), oral cavity (3), oropharynx (2), nasopharynx (1)	
	Lymphoma (4)	Oropharynx (2), cervical lymph node (2)	
	Nasopharyngeal carcinoma (2)	Nasopharynx (2)	
	Laryngeal carcinoma (2)	Larynx (2)	
	Carcinoma metastasis (2)	Deep cervical spaces (2)	
	Malignant mesenchymal tumor (2)	Larynx (2)	
	Neuroendocrine tumor (1)	Parotid gland (1)	
	Follicular carcinoma (1)	Thyroid gland (1)	
	Oncocytic mucoepidermoid carcinoma (1)	Parotid gland (1)	
	Malignant melanoma (1)	Oral cavity (1)	
Papillary thyroid carcinoma (1)	Thyroid gland (1)		
Benign lesions (n=28)	Inflammatory (n=14)	Chronic inflammation (7)	Parapharyngeal spaces (3), submandibular lymph node (2), nasopharynx (1), oral cavity (1)
		Granulomatous inflammation (4)	Cervical lymph node (2), parotid gland (1), submandibular lymph node (1)
		Sialadenitis (2)	Parotid gland (2)
		Lymphocytic thyroiditis (1)	Thyroid gland (1)
	Noninflammatory (n=14)	Pleomorphic adenoma (3)	Parotid gland (3)
		Lymphoid hyperplasia (2)	Palate (2)
		Warthin tumor (2)	Parotid gland (2)
		Benign mixed tumor (2)	Parotid gland (2)
		Hemangioma (2)	Oral cavity (2)
		Peripheral giant cell granuloma (1)	Maxillary space (1)
Keratinous cyst (1)	Subcutaneous space (1)		
Benign peripheral nerve sheath tumor (1)	Parotid gland (1)		

Number of lesions are given within parentheses.

was used for calculation of ADC values. The ADC measurements were calculated on ADC maps which were generated from DW-MRI with b=1000 s/mm². We used a region of interest (ROI) with a median size of 30 mm² to calculate the ADC values on ADC maps. In patients with more than one lesion with the same pathology, ADC measurement was obtained from the largest lesion. We measured three ROIs with similar size from the solid portion of the mass to obtain a mean ADC value corresponding to the contrast-enhanced T1-weighted image. We avoided necrotic

or cystic parts of the tumors illustrated on the corresponding T2-weighted image. Radiologists performing the measurements were blinded to the histopathological results.

We also measured ADC value of spinal cord and cerebrospinal fluid (CSF) in the upper neck area to assess the validity and standardization of our method, due to the variety of localization and histopathological diagnosis of lesions.

Histopathologic classification

The diagnosis and location of lesions are given in Table 1. Definitive

Table 2. Median ADC value of the head and neck lesions

Head and neck lesions	Median ADC (min–max) ($\times 10^{-3}$ mm ² /s)	<i>P</i> *
Benign	1.17 (0.52–2.38)	<0.001
Malignant	0.72 (0.39–1.51)	
Malignant		
SCC	0.73 (0.65–1.06)	0.799
Non-SCC	0.74 (0.63–1.51)	
Benign		
Inflammatory	1.14 (0.85–2.38)	0.910
Noninflammatory	1.27 (0.52–2.33)	

ADC, apparent diffusion coefficient; SCC, squamous cell carcinoma.
*Mann Whitney U test.

classified as inflammatory (n=14) and noninflammatory (n=14).

Statistical analysis

SPSS 19.0 (IBM Corp.) was used for statistical analysis. Descriptive statistics of continuous variables are given as mean, standard deviation, median, minimum, and maximum values. Categorical variables are presented as frequency and percent. Shapiro Wilk test was used for test of normality. Mann Whitney U test was used for nonparametric two group comparisons. Receiver operating characteristic (ROC) analysis was used with Youden Index to find a cutoff value for benign and malignant discrimination. For all statistical comparisons $P < 0.05$ was assumed to be statistically significant.

Results

The median ADC value of the malignant tumors and benign lesions were 0.72×10^{-3} mm²/s, (range, $0.39\text{--}1.51 \times 10^{-3}$ mm²/s) and 1.17×10^{-3} mm²/s (range, $0.52\text{--}2.38 \times 10^{-3}$ mm²/s), respectively. There was a significant difference between ADC value of benign and malignant lesions ($P < 0.001$) (Table 2).

ROC analysis was used to detect the cutoff point differentiating malignant lesions from benign pathologies (Fig. 1). The area under the curve was larger than 0.83 ($P < 0.001$). When 0.98×10^{-3} mm²/s was used as the cutoff ADC to distinguish between benign and malignant lesions, sensitivity was calculated as 85.3% and specificity as 78.6%.

Among malignant lesions, the lowest median ADC value was calculated in lymphoma patients (n=4) as 0.44×10^{-3} mm²/s (range, $0.39\text{--}0.58 \times 10^{-3}$ mm²/s) (Fig. 2). SCC, the most common malignant head and neck tumor (n=17), had a median ADC value of 0.72×10^{-3} mm²/s (range, $0.65\text{--}1.06 \times 10^{-3}$ mm²/s) (Fig. 3). ADC values of lymphoma and SCC patients were significantly different ($P < 0.001$).

When carcinomas of head and neck were divided into SCC and non-SCC groups, the median ADC value of non-SCC group tumors (n=13) was 0.74×10^{-3} mm²/s (range, $0.63\text{--}1.51 \times 10^{-3}$ mm²/s). There was no significant difference between ADC value of these tumors ($P = 0.799$) (Table 2).

When SCC patients were divided in three groups according to their

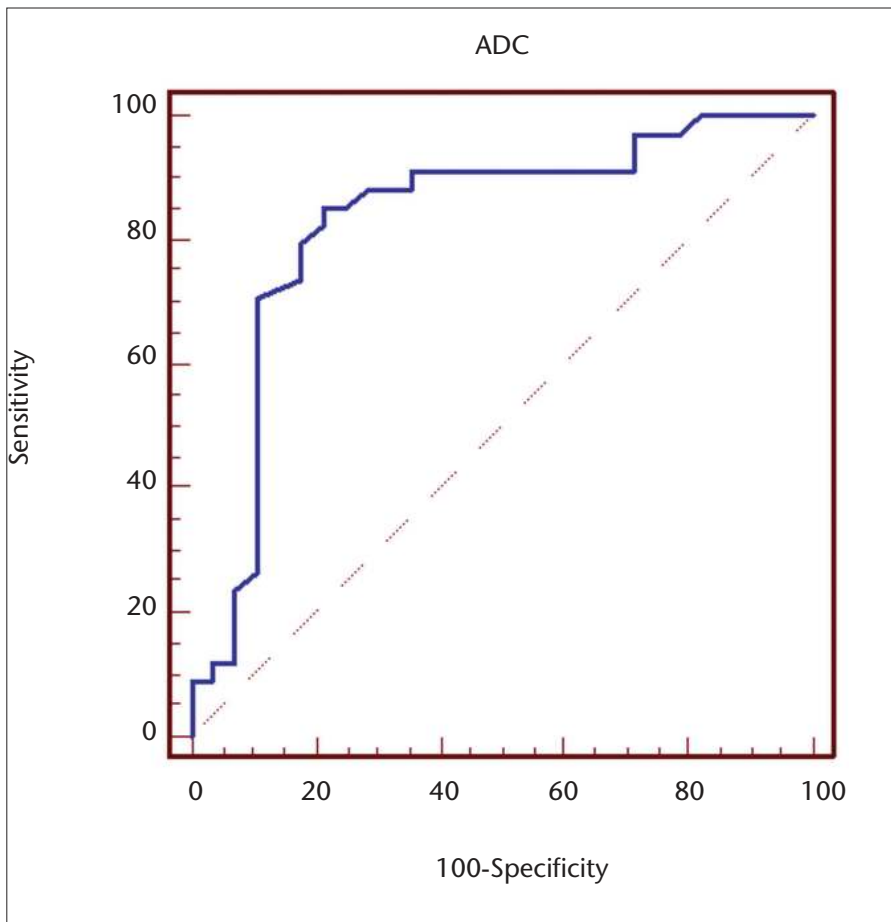


Figure 1. Receiver operating characteristic (ROC) curve of the ADC value used for differentiating malignant tumors from benign lesions. The area under the curve (AUC) is 0.83.

histopathological diagnosis was made following surgical operation in 35 patients, by tru-cut biopsy in 16 patients, and by thin-needle biopsy in 11 patients. Lesions were classified into two main groups: benign (n=28) and malignant (n=34). Malignant lesions were

classified as lymphoma (n=4) and carcinoma (n=30). Squamous cell carcinoma (SCC) patients was classified according to the level of differentiation as well-differentiated (n=4), moderately differentiated (n=9) and poorly differentiated (n=4). Benign lesions were

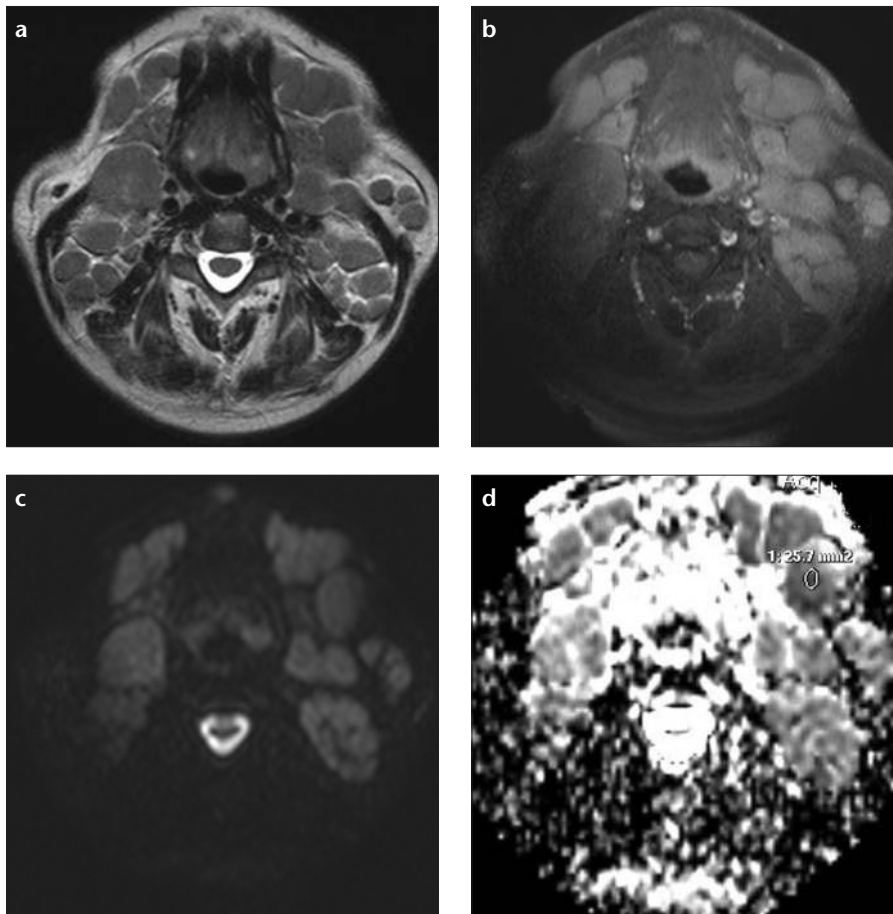


Figure 2. a–d. Transverse MR images of a 67-year-old male patient with B cell lymphoma. T2-weighted image (a) shows multiple enlarged cervical lymph nodes. In T1-weighted fat-suppressed postcontrast image (b), cervical lymph nodes were slightly enhanced. DW-MRI (c) shows increased signal intensity of the cervical lymph nodes. The ADC map (d) shows low signal intensity in the lymph nodes (median ADC, $0.35 \times 10^{-3} \text{ mm}^2/\text{s}$).

Table 3. Median and mean ADCs of the lesions, spinal cord, and CSF

Diagnosis	ADC of lesion Median (min–max) ($\times 10^{-3} \text{ mm}^2/\text{s}$)	ADC of the spinal cord Mean \pm SD ($\times 10^{-3} \text{ mm}^2/\text{s}$)	ADC of CSF Median (min–max) ($\times 10^{-3} \text{ mm}^2/\text{s}$)
Inflammatory	0.14 (0.85–2.38)	0.79 ± 0.10	3.30 (2.73–4.84)
Noninflammatory	1.27 (0.52–2.33)	0.77 ± 0.11	3.23 (2.25–3.71)
SCC	0.73 (0.65–1.06)	0.79 ± 0.10	3.08 (2.37–3.65)
Non-SCC	0.72 (0.39–1.51)	0.77 ± 0.10	3.23 (3.03–3.62)
<i>P</i>	<0.001 ^a	0.841 ^b	0.498 ^a

Normally distributed variables are given as mean and standard deviation; non-normally distributed variables are given as median, minimum, and maximum.

ADC, apparent diffusion coefficient; CSF, cerebrospinal fluid; SCC, squamous cell carcinoma.

^aOne-way ANOVA.

^bKruskal Wallis test.

histopathological differentiation, the median ADC value for well-, moderately, and poorly differentiated SCC were $0.94 \times 10^{-3} \text{ mm}^2/\text{s}$ (range, $0.7\text{--}1.06 \times 10^{-3} \text{ mm}^2/\text{s}$), $0.72 \times 10^{-3} \text{ mm}^2/\text{s}$ (range, $0.68\text{--}1.07 \times 10^{-3} \text{ mm}^2/\text{s}$), and $0.8 \times 10^{-3} \text{ mm}^2/\text{s}$ (range, $0.64\text{--}0.96 \times 10^{-3}$

mm^2/s), respectively. To compare our findings with results of a previous study we divided SCC in two groups according to histopathological differentiation: well- or moderately differentiated SCC ($n=13$) and poorly differentiated SCC ($n=4$). Median ADC was

$0.83 \times 10^{-3} \text{ mm}^2/\text{s}$ (range, $0.65\text{--}1.06 \times 10^{-3} \text{ mm}^2/\text{s}$) for well- or moderately differentiated SCCs. ADC values were not significantly different between the two groups ($P = 0.350$).

In benign lesions, the median ADC value of inflammatory and noninflammatory lesions were $1.13 \times 10^{-3} \text{ mm}^2/\text{s}$ (range, $0.85\text{--}2.38 \times 10^{-3} \text{ mm}^2/\text{s}$) and $1.27 \times 10^{-3} \text{ mm}^2/\text{s}$ (range, $0.52\text{--}2.33 \times 10^{-3} \text{ mm}^2/\text{s}$), respectively. The ADC value of inflammatory lesions did not significantly differ from those of noninflammatory benign lesions ($P = 0.910$) (Table 2).

No significant differences in the mean and median ADCs of the spinal cord and CSF were seen among four categories (Table 3). The mean and median ADCs of the spinal cord and CSF in all 62 patients were $(0.77 \pm 0.10) \times 10^{-3} \text{ mm}^2/\text{s}$ and $3.24 (2.25\text{--}4.84) \times 10^{-3} \text{ mm}^2/\text{s}$, respectively.

Discussion

There are very few studies in the literature on the use of DW-MRI for benign neck pathologies and inflammatory diseases (12, 13). Kito et al. (13) studied neck abscess and found that the ADC values in those with abscess and inflammation were statistically and significantly lower than the ADC values of those with normal tissue in the oral and maxillofacial region. They showed that the protein complexes in the necrotic parts of the inflammatory lesions and possible presence of microorganisms with inflammatory cells limit the diffusion of water molecules, and as a result, lower ADC values were obtained. According to the study of Kito et al. (13), it is possible to distinguish inflammatory and non-inflammatory tissues using DW-MRI, without contrast material. In the current literature, there has been no study comparing the differences between ADC values of inflammatory and non-inflammatory head and neck lesions. In our study, we separated benign lesions as inflammatory and noninflammatory benign lesions. The median ADC value of inflammatory lesions ($1.13 \times 10^{-3} \text{ mm}^2/\text{s}$) was lower than the median ADC value of noninflammatory benign lesions ($1.26 \times 10^{-3} \text{ mm}^2/\text{s}$), but there was no statistically significant difference between the ADC values of the two groups. This may be be-

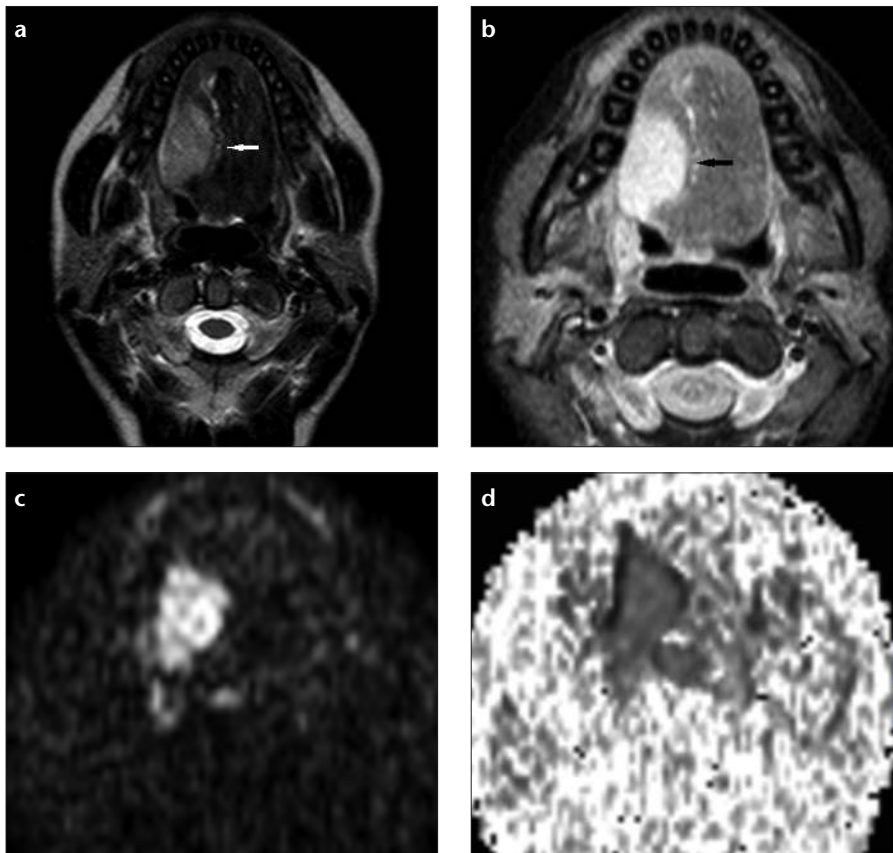


Figure 3. a–d. Squamous cell carcinoma in the base of the tongue in a 19-year-old woman. T2-weighted transverse image (a) shows a hyperintense mass on the right-side of the tongue (white arrow). T1-weighted fat-suppressed postcontrast transverse image (b) shows marked enhancement (black arrow). DW-MRI (c) shows the mass as having a high signal intensity. The ADC map (d) shows low signal intensity in the mass (ADC value, $0.79 \times 10^{-3} \text{ mm}^2/\text{s}$).

cause benign mass lesions are regarded as noninflammatory in our study unlike previous studies in which normal tissues are regarded as noninflammatory. As a result, the wide histopathological variety among noninflammatory benign lesions affected our results. We believe that more studies are required to evaluate the ADC values of inflammatory lesions.

The ADC values of malignant neck lesions have been found to be lower than benign lesions by a significant rate in many studies (9, 11, 14). This situation is linked to the histopathological differences between benign and malignant lesions.

Wang et al. (9) reported that the threshold ADC value of $1.22 \times 10^{-3} \text{ mm}^2/\text{s}$ had 84% sensitivity and 91% specificity for differentiation of benign-malignant masses. Sasaki et al. (14) compared ADC values in a study of sinonasal masses and found that ADC values above $0.84 \times 10^{-3} \text{ mm}^2/\text{s}$ had 61% sensitivity

and 94% specificity for benign lesions. Similarly, Abdel Razek et al. (11) found $1.25 \times 10^{-3} \text{ mm}^2/\text{s}$ ADC value had a sensitivity of 94% and a specificity of 91% for benign-malignant mass differentiation in a study of head and neck masses in pediatric patients. Sakamoto et al. (15) used a threshold ADC value of $1.61 \times 10^{-3} \text{ mm}^2/\text{s}$ and contrary to the previous literature they found that there was no statistical difference between the ADC values of benign and malignant masses. This was linked to the wide range of variations in ADC values due to tumor cellularity, cystic or necrotic component and presence of fibrosis. Our study agrees with most studies in the literature with a statistically significant difference between the ADC values of benign and malignant tumors. The $0.961 \times 10^{-3} \text{ mm}^2/\text{s}$ cutoff value determined in our study had 81.25% sensitivity and 78.57% specificity to distinguish benign versus malignant head and neck masses.

The reason for our lower specificity was due to the wide histopathological variety in the benign mass group. Especially, the low ADC values of Warthin tumor ($n=2$, mean ADC, $1.05 \times 10^{-3} \text{ mm}^2/\text{s}$) played a role in reducing specificity (Fig. 4). In the studies of Abdel Razek et al. and Sasaki et al. (11, 14) there was no Warthin tumor and ADC values of benign lesions were relatively homogeneous. The ADC values of Warthin tumors were shown to be low in studies comparing benign salivary gland lesions such as pleomorphic adenoma and Warthin tumor (16, 17).

In our study, when malignant lesions were compared, the average ADC value of lymphoma patients ($0.44 \times 10^{-3} \text{ mm}^2/\text{s}$) was found to be significantly lower than that of SCC and other malignant group patients, in line with other studies in the literature (9, 10, 14, 18). In a study by Wang et al. (9), the average ADC values of carcinoma group patients (SCC and adenocarcinoma) were significantly higher than the average ADC values of the lymphoma patients. High ADC values in the carcinoma group were linked to the presence of necrotic foci which are too small to be identified on MRI. On the other hand, Maeda et al. (10) stated that many small necrosis foci would be smaller than the voxel size of the MRI and as a result they would not change the ADC values, contradicting the conclusion of Wang et al. (9). Instead, they linked this difference to the high cellularity of lymphoma. Ichikawa et al. (19) stated that ADC-based differentiation between lymphomas and oropharyngeal carcinomas was possible. However, they reported that discrimination of nasopharyngeal carcinomas from lymphoma based on ADC values was not effective due to histological similarity of nasopharyngeal carcinomas and lymphomas.

When the SCC patient group was compared based on the degree of differentiation, different results were obtained in many earlier studies (9, 10, 20). Wang et al. (9) reported that the ADC values of poorly differentiated SCC patients were significantly lower compared to the ADC values of moderately and well-differentiated SCC patients. Sumi et al. (20) found that

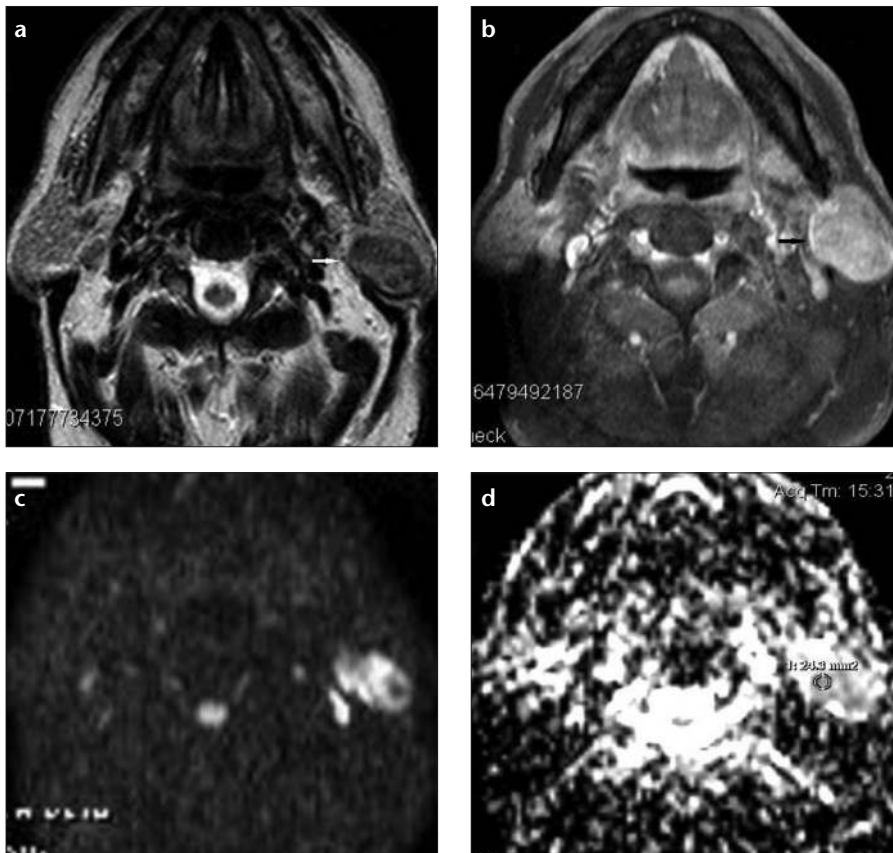


Figure 4. a–d. Transverse MR images of a 63-year-old male patient with left parotid gland Warthin tumor. T2-weighted image (a) shows a hypointense mass compared with the parotid gland parenchyma (white arrow). T1-weighted fat-suppressed postcontrast image (b) shows moderate enhancement in the left parotid gland mass (black arrow). DW-MRI (c) shows a high signal intensity mass in the left parotid gland. The ADC map (d) shows heterogeneous low signal intensity in the tumor area (ADC value, $0.81 \times 10^{-3} \text{ mm}^2/\text{s}$).

the ADC values of well- and moderately differentiated SCC patients were significantly higher compared to those of poorly differentiated patients. Maeda et al. (10) reported that the average ADC values of the well- and moderately differentiated group were not significantly different from those of the poorly differentiated SCC patients. SCC differentiation is linked to the degree of keratinization, cell atypia, and stratification, which are compared qualitatively to distinguish the subtypes. Poorly differentiated SCC has more cell atypia compared to the other groups. As cell atypia increases, water molecule diffusion is limited and thus ADC values decrease. The effects of histological features such as

the keratinization and cellular atypia to ADC values cannot be estimated. SCCs show heterogeneous histological differentiation and therefore histological section does not always correlate with DW-MRI maps.

There were several limitations in our study. First, to avoid selection bias and reflect the efficacy of DW-MRI on daily routine, we included patients of various ages, with involvement of different neck regions and different pathological diagnoses. Some pathology groups included a small number of patients. Additionally, sensitivity to susceptibility artifacts is relatively higher in our study because we used EPI DW-MRI. Use of more rapid sequences (SENSE, HASTE, etc.) instead of EPI DW-MRI would have reduced the sensitivity to these artifacts. Lastly, lesions under 1 cm diameter were excluded from our study to avoid susceptibility artifacts. Future studies using rapid DW-MRI

techniques are required to evaluate smaller head and neck lesions.

In conclusion, DW-MRI with quantitative ADC values may help to differentiate and characterize benign and malignant head and neck lesions.

Conflict of interest disclosure

The authors declared no conflicts of interest.

References

1. Driessen JP, van Kempen PM, van der Heijden GJ, et al. Diffusion-weighted imaging in head and neck squamous cell carcinomas: A systematic review. *Head Neck* 2015; 37:440–448. [CrossRef]
2. Yoshino N, Yamada I, Ohbayashi N, et al. Salivary glands and lesions: evaluation of apparent diffusion coefficients with split-echo diffusion-weighted MR imaging—initial results. *Radiology* 2001; 221:837–842. [CrossRef]
3. Sakamoto J, Sasaki Y, Otonari-Yamamoto M, Sano T. Comparison of various methods for quantification of apparent diffusion coefficient of head and neck lesions with HASTE diffusion-weighted MR imaging. *Oral Surg Oral Med Oral Pathol Oral Radiol* 2012; 114:266–276. [CrossRef]
4. Kim YJ, Chang KH, Song IC, et al. Brain abscess and necrotic or cystic brain tumor: discrimination with signal intensity on diffusion-weighted MR imaging. *AJR Am J Roentgenol* 1998; 171:1487–1490. [CrossRef]
5. Schaefer PW. Applications of DWI in clinical neurology. *J Neurol Sci* 2001; 186:S25–S35. [CrossRef]
6. Moseley ME, Kucharczyk J, Mintorovitch J, et al. Diffusion-weighted MR imaging of acute stroke: correlation with T2-weighted and magnetic susceptibility-enhanced MR imaging in cats. *AJNR Am J Neuroradiol* 1990; 11:423–429.
7. Trojanowska A. Squamous cell carcinoma of the head and neck—The role of diffusion and perfusion imaging in tumor recurrence and follow-up. *Rep Prac Oncol Radiother* 2011; 16:207–212. [CrossRef]
8. Varoquaux A, Rager O, Lovblad KO, et al. Functional imaging of head and neck squamous cell carcinoma with diffusion-weighted MRI and FDG PET/CT: quantitative analysis of ADC and SUV. *Eur J Nucl Med Mol Imaging* 2013; 40:842–852. [CrossRef]
9. Wang J, Takashima S, Takayama F, et al. Head and neck lesions: characterization with diffusion-weighted echo-planar MR imaging. *Radiology* 2001; 220:621–630. [CrossRef]
10. Maeda M, Kato H, Sakuma H, Maier SE, Takeda K. Usefulness of the apparent diffusion coefficient in line scan diffusion-weighted imaging for distinguishing between squamous cell carcinomas and malignant lymphomas of the head and neck. *AJNR Am J Neuroradiol* 2005; 26:1186–1192.
11. Abdel Razek AK, Gaballa G, Elhawary G, Megahed AS, Hafez M, Nada N. Characterization of pediatric head and neck masses with diffusion-weighted MR imaging. *Eur Radiol* 2009; 19:201–208. [CrossRef]

12. Maeda M, Maier SE. Usefulness of diffusion-weighted imaging and the apparent diffusion coefficient in the assessment of head and neck tumors. *J Neuroradiol* 2008; 35:71–78. [\[CrossRef\]](#)
13. Kito S, Morimoto Y, Tanaka T, et al. Utility of diffusion-weighted images using fast asymmetric spin-echo sequences for detection of abscess formation in the head and neck region. *Oral Surg Oral Med Oral Pathol Oral Radiol Endod* 2006; 101:231–238. [\[CrossRef\]](#)
14. Sasaki M, Eida S, Sumi M, Nakamura T. Apparent diffusion coefficient mapping for sinonasal diseases: differentiation of benign and malignant lesions. *AJNR Am J Neuroradiol* 2011; 32:1100–1106. [\[CrossRef\]](#)
15. Sakamoto J, Yoshino N, Okochi K, et al. Tissue characterization of head and neck lesions using diffusion-weighted MR imaging with SPLICE. *Eur J Radiol* 2009; 69:260–268. [\[CrossRef\]](#)
16. Ikeda M, Motoori K, Hanazawa T, et al. Warthin tumor of the parotid gland: diagnostic value of MR imaging with histopathologic correlation. *AJNR Am J Neuroradiol* 2004; 25:1256–1262.
17. Yabuuchi H, Matsuo Y, Kamitani T, et al. Parotid gland tumors: can addition of diffusion-weighted MR imaging to dynamic contrast-enhanced MR imaging improve diagnostic accuracy in characterization? *Radiology* 2008; 249:909–916. [\[CrossRef\]](#)
18. Fatima Z, Ichikawa T, Ishigame K, et al. Orbital masses: the usefulness of diffusion-weighted imaging in lesion categorization. *Clin Neuroradiol* 2014; 24:129–134. [\[CrossRef\]](#)
19. Ichikawa Y, Sumi M, Sasaki M, et al. Efficacy of diffusion-weighted imaging for the differentiation between lymphomas and carcinomas of the nasopharynx and oropharynx: correlations of apparent diffusion coefficients and histologic features. *AJNR Am J Neuroradiol* 2012; 33:761–766. [\[CrossRef\]](#)
20. Sumi M, Sakihama N, Sumi T, et al. Discrimination of metastatic cervical lymph nodes with diffusion-weighted MR imaging in patients with head and neck cancer. *AJNR Am J Neuroradiol* 2003; 24:1627–1634.